ACS OMEGA

Open Access

http://pubs.acs.org/journal/acsodf

Article

Polyaniline/Titania Nanotube-Based Biosensor Strip for Sensitive and Specific Electrochemical Detection of SARS-CoV-2

Al-mahmnur Alam, Timsy Uppal, Md Shariful Islam, Manoranjan Misra,* and Subhash C Verma*

Cite This: *ACS Omega* 2023, 8, 45700−45707

Read Online

ACCESS | Metrics & More | Article Recommendations | Supporting Information

ABSTRACT: This study showcases the creation of a biosensor strip designed for the rapid, precise, and highly sensitive electrochemical detection of severe acute respiratory syndrome coronavirus 2 (SARS-CoV-2). These biosensor strips were crafted by affixing a monoclonal antibody (mAb) specific to SARS-CoV-2 onto the surface of a commercially screen-printed carbon electrode (SPCE) modified with polyaniline-titania nanotubes (PANi-TNT). The transportable sensing device was constructed by pairing the mAb functionalized strip with a portable potentiostat wirelessly connected to either a Windows or Android device. Fast and specific conjugation between spike protein of SARS-CoV-2 and immobilized anti-SARS-CoV-2 triggered a change in the charge and electron mobility in the biosensing layer of the strip to produce detectable current during chronoamperometric scanning in the presence of a phosphate buffer solution (PBS). The excellent sensitivity and specificity of the sensor toward SARS-CoV-2 were detected as analytical analysis demonstrated linearity in the range of 80 to 200 copies/μL with a limit of detection of 25.59 copies/μL from the dose−response and standard fitted curve. Through experimental validation, the sensor strip's ability to specifically detect SARS-CoV-2 was established, distinguishing it from human coronavirus-OC43 (HCoV-OC43), HCoV-NL63, HCoV-229E, and adenovirus. The results from these tests indicate that these strips possess the potential for the future creation of dependable and easily transportable point-of-care diagnostic devices, enabling swift, sensitive, and precise detection of SARS-CoV-2 in the saliva or nasopharyngeal fluid of individuals infected with the virus.

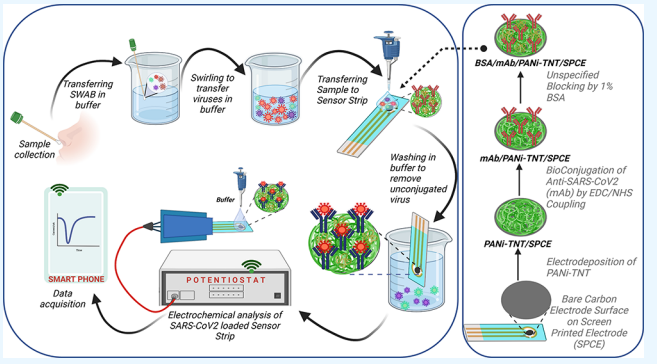

1. INTRODUCTION

Since the emergence of the novel coronavirus (COVID-19) in Wuhan, China, in 2019, there has been an ongoing effort to develop swift and precise SARS-CoV-2 detection devices in the manufacturing sector.[1] In the current landscape of rapid SARS-CoV-2 testing, a wide range of methodologies have surfaced, including the identification of various targets, such as RNA, antibodies, and antigens. The foremost approach extensively employed for the screening and early diagnosis of SARS-CoV-2 is the quantitative reverse transcription polymerase chain reaction (qRT-PCR) method.[2] Typically, qRT-PCR establishes higher sensitivity, accuracy, and reliability for the detection of viral RNA with a limit of detection (LOD) of a few viral RNA copies.[3,4] Despite this, it demands certified laboratories with expensive equipment, trained technicians, and a longer processing time of at least several hours.[5−7]

Rapid, facile, cost-effective, and available detection for large-scale screening, in-field testing, and point-of-care (POC) diagnosis of the disease is essential to identify and isolate the COVID-19-positive patient from a healthy individual to control highly contagious SARS-CoV-2. In this context, direct detection of viral proteins (antigens) is advantageous in clinical samples such as saliva or nasal fluid without complicated sample preparation steps for large-scale screening. It is reported that SARS-CoV-2 exists in the saliva of almost all COVID-19 patients.[4] However, saliva comprises many proteins, such as immunoglobulins, mucins, enzymes, hormones, electrolytes, and metabolites. Therefore, a strategy to detect SARS-CoV-2 antigens with high sensitivity and specificity in noninvasive samples such as saliva through POC diagnosis is critical in controlling the spread of the deadly coronavirus.

Biosensor-based POC screening is a practical option to adopt in this crisis for faster diagnosis of SARS-CoV-2 covering surface antigens, whole viruses, antibodies, and potential breath-bound biomarkers.[8,9] Depending on the transduction mechanism, they can be classified into electrochemical, optical, calorimetric, piezoelectric, and thermoelectric.[10] However,

Received: August 18, 2023
Revised: October 28, 2023
Accepted: November 2, 2023
Published: November 22, 2023

electrochemical biosensors with miniaturized features for POC screening are extremely trendy because of rapid response time, high sensitivity of detection, simplicity of fabrication, portability, and user-friendliness.[11] Frequent reports of electrochemical biosensors, including amperometric, potentiometric, voltammetric, impedimetric, or field-effect transistors, have been available to detect SARS-CoV-2 since 2019.[12] The success of biosensors depends on the accuracy and precision of processing the electrochemical change that occurred during interactions of the receptor−analyte on the biosensor chip. Therefore, the functionality of biosensors immensely depends on the materials or sensing component.[13,14] Nanomaterials, including nanoparticles, quantum dots, nanowires, and nanotubes, have been extensively explored as sensing elements because they possess unique physical and chemical properties due to high surface area, nanoscale size, and tunable electrical, optical, or magnetic characteristics.[15−18] It was realized that nanomaterials perform remarkably to enhance the electrochemical reaction rate by increasing the electrode surface area-to-volume ratio, thereby increasing the electrode surface area to analyte fluid volume.[19−22] It was noticed over the decades that carbonaceous (graphene and carbon nanotube), metal (gold, silver, platinum, copper, etc.), ceramic, polymeric, and semiconductor materials were studied extensively to fabricate biosensors for specific detection of virus antigens including influenza virus, avian influenza H5N1, chikungunya virus DNA, influenza virus H9N2, influenza virus H1N1, hepatitis B antigen, hepatitis C virus core antigen, and SARS-CoV-2.[23−30]

In recent years, several nanostructure-modified screen-printed carbon electrodes (SPCEs) have been reported to fabricate biosensors for the detection of COVID-19, for instance, SPCE with molecularly imprinted polymer nanomaterials (MIP),[31] Whatman chromatographic paper-based biosensor strip containing recombinant SARS-CoV-2 nucleocapsid antigen,[32] gold/graphene nanohybrids on SPCE modified by polyarginine and MIP,[33] gold nanoparticles on SPCE and immobilized antibody,[34] *para*-aminobenzoic acid on SPCE and immobilized monoclonal SARS-CoV-2 antibody,[35] gold nanoparticles on SPCE modified with an aptamer,[36] phytic acid-doped polyaniline film on SPCE to immobilize recombinant spike protein,[37] and stencil-printed carbon electrode capturing antibodies modified by horseradish peroxidase.[38]

In this study, we have reported a blended matrix of polyaniline (PANi) and titania nanotube (TNT)-modified SPCE for the development of a monoclonal antibody (mAb) anti-SARS-CoV-2-immobilized chronoamperometric (CA) biosensor strip. A commercial SPCE as a transducer in an electrochemical biosensor offers a great deal of miniaturizing diagnosis processes to commercialize POC devices. However, the integration of a nanostructure into the SPCE opens a new possibility to enhance the efficiency of biosensing. The blending of TNT with PANi has made the SPCE more robust and conductive because of its semiconducting properties and biocompatibility. Our previous studies have reported cobalt (Co)-functionalized TNT sensor chips to detect the sRBD of SARS-CoV-2 and biomarkers associated with tuberculosis.[20] The general mechanism involves the formation of a complex between Co and the specific biomarker or sRBD of SARS-CoV-2 at a particular bias voltage due to the reduction of Co^{2+} ions and oxidation of the analyte.[19,21]

We demonstrate that an anti-SARS-CoV-2-loaded PANi-TNT-based sensor strip can achieve an LOD of as low as 25.59 copies/μL of SARS-CoV-2 in human saliva and can be a potential candidate for the POC-based diagnosis toward rapid detection of SARS-CoV-2.

2. RESULTS AND DISCUSSION

2.1. Physio-Electrochemical Characterization of the Modified SPCE. The stepwise surface modification of the SPCE, progressing from its initial bare state to the subsequent bioconjugation with the mAb, was evaluated through the examination of surface morphology and the alterations in the electrochemical properties of the strips. The left panel of Figure 1 demonstrates the noticeable change of the working

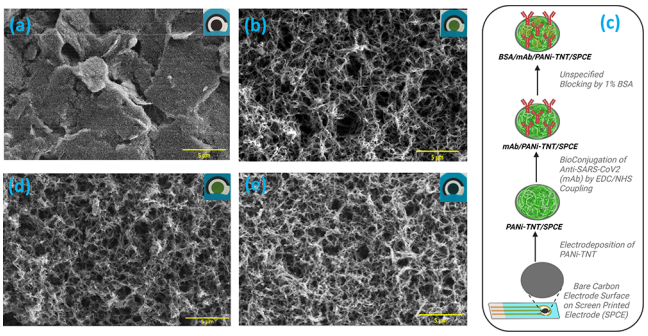

Figure 1. (Left panel) Surface morphology of the (a) bare SPCE, (b) PANi/SPCE, (d) PANi-TNT/SPCE, and (e) anti-SARS-CoV-2/PANi-TNT/SPCE (scale bar 5 μm). Schematic illustration at the right panel (c) of the modification of the WE (SPCE) surface by coelectropolymerization of a blend of aniline and TNT and the immobilization procedure of anti-SARS-CoV-2 on the modified surface of the SPCE.

electrode (WE) surface of the bare SPCE (a), PANi-modified SPCE (PANi/SPCE) (b), PANi-TNT-modified SPCE (PANi-TNT/SPCE) (d), and antibody-immobilized anti-SARS-CoV-2/PANi-TNT/SPCE (e). The optical images of the SPCE also reflect the step-by-step modification of the WE as the color changes from black to green to dark green due to functionalization by the metal, polymer, and biomolecule (Figure 1a−b, d−e). The SEM imaging uncovers the presence of the backbone of this sensor strip, PANi as a wide and well-distributed fibrous network on the WE of the SPCE in Figure 1b−d. TNT was added as an additive along with PANi to enhance the conductivity of the sensing platform.

In the beginning, the blend of PANi-TNT was electrodeposited on the WE by coelectropolymerization of an acidic mixture of aniline and TNT. The SEM imaging revealed that both 5 (Figure S1b) and 10 cycles (Figure S2b) of CV scanning at 50 mVs^{-1} were good enough to decorate the surface of the WE by PANi-TNT to grow a uniform fibrous network. However, 10 cycles of CV scan caused the imprecise aggregation of either TNT or PANi across the surface of the WE (Figure S2b). On the contrary, the uniform distribution of the PANi-TNT fibrous network on the SPCE with less aggregation was visualized from the 5 cycles of CV (Figure S1b). This condition was, therefore, applied throughout the surface modification of the WE. The thickness of the PANi-TNT layer was calculated to be 2−4 μm from the cross-sectional surface image of the sample obtained after 5 cycles of CV scan, as seen in Figure S1c. Energy-dispersive X-ray spectroscopy (EDX) analysis along with SEM imaging confirmed the presence of titania and the composition of

https://doi.org/10.1021/acsomega.3c06133
ACS Omega 2023, 8, 45700−45707

another possible atom in the matrix, as illustrated in Figure S4. Electrochemical studies of PANi/SPCE and PANi-TNT/SPCE were performed in the presence of 0.1 M HCl to justify the inclusion of TNT with the PANi network in support of the enhancement of the conductivity of the sensor. According to the CV in Figure 2a, PANi/SPCE exhibited a typical redox pair

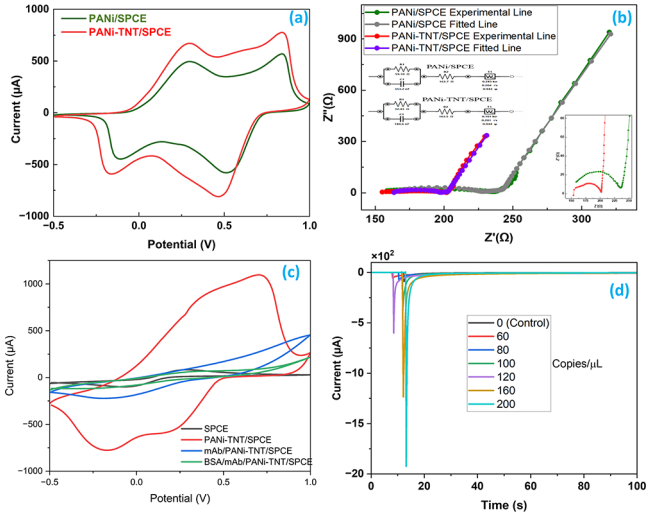

Figure 2. (a) CV of the PANi/SPCE (green) and PANi-TNT/SPCE (red); (b) Nyquist plot of the experimental and fitted results with inset images of the Nyquist plot of the PANi/SPCE (green) and PANi-TNT/SPCE (red); (c) CV of the sensor strip during the modification of the SPCE by PANi-TNT, anti-SARS-CoV-2, and SARS-CoV-2 in 0.5 mM potassium ferrocyanide/potassium ferricyanide in 0.01 M PBS buffer at a scan rate of 50 mVs^{-1}; (d) signal output of different concentrations (copies/μL) of inactivated SARS-CoV-2 at the potentiostat during CA scanning at a −0.2 bias voltage.

of PANi where the first redox peak at 0.46/−0.28 V relates to the leucoemeraldine (LE) transition to the partly oxidized emeraldine and the second redox peak (0.89/0.5 V) can be ascribed to the (E) transition to the entirely oxidized pernigraniline (PA). The CV of PANi-TNT/SPCE also shows two pairs of clear redox couples that follow the pseudocapacitive behavior of PANi. However, it was noticed that a higher redox peak current is observed in the PANi-TNT/SPCE than in the PANi/SPCE. This observation implies the fast electron exchange behavior and electrocatalytic activity[39,40] of the sensing platform due to the higher transfer rate in the presence of TNT.[41,42] To support this study, an electrochemical impedance spectroscopy experiment and analysis were performed, and modified Randles equivalent circuits for both PANi/SPCE and PANi-TNT/SPCE were fitted, which are shown in Figure 2b. The Nyquist plots of both the PANi/SPCE and PANi-TNT/SPCE exhibit a semicircle of higher and lower diameters, respectively, in the high-to-medium frequency range, corresponding to the charge transfer resistance (R_{ct}) at the electrode/electrolyte interface, followed by a straight line in the low-frequency region, which stands for the Warburg diffusion impedance and relates to the bulk diffusion resistance in the hybrid model.[41,42] In addition, the solution resistances for both the PANi/SPCE and PANi-TNT/SPCE are the same (R_2 = 163.7 and 163.5 Ω, respectively) in the equivalent circuits. The R_{ct} (R_1 in the modified Randles equivalent circuit) values of the PANi/SPCE and PANi-TNT/SPCE are found to be 65 and 32 Ω, respectively. The mean errors for charge transfer impedance and solution resistance values determined by modified Randles circuit fitting are 2.79 and 0.78%, respectively, which show consistency between experimental and fitted data. The lower R_{ct} value of the PANi-TNT/SPCE is because of the presence of TNT, which enables redox couple adsorption and enrichment on the WE surface,[39] implying better electronic transport and conductivity,[43] which is an important prerequisite to constructing a fast, sensitive, and robust biosensing platform reliable POC device to quantify target viral pathogens.

Likewise, SEM imaging of the PANi-TNT/SPCE surface after the immobilization of anti-SARS-CoV-2 demonstrates the uniform distribution of the mAb on the entire surface, as seen in Figure 1d. In a previous analysis (Figure S3b), it was noticed that a higher concentration (5.00×10^{-3} $\mu g/\mu L$) of the antibody had caused a noticeable aggregation on the surface of the PANi-TNT/SPCE, which is detrimental toward the target "sensing and antibody-antigen" application. It was assumed that the abundant terminal $-NH_2$ group of PANi has put up strong covalent bonding (amide formation) with the available activated-carboxylic group of antibodies in the presence of EDC/NHS.[44] On the contrary, the excess antibody has been physically adsorbed on top of the chemically attached antibody and caused aggregation on the surface. However, the uniform coverage of the antibody was obtained from the 2.45×10^{-3} $\mu g/\mu L$ of anti-SARS-CoV-2 (Figure S3a), which has been used to further immobilization.

A set of CV scanning was performed to understand the electrochemical behavior of anti-SARS-CoV-2/PANi-TNT/SPCE after each stage of modification in the presence of 5 mM potassium ferrocyanide/potassium ferricyanide in 0.1 M PBS buffer. As shown in Figure 2c, a pair of well-defined redox peaks were observed from the bare SPCE. A modified shape of the anodic peak at 0.6 V and the cathodic one at −0.2 V with enhanced intensity was observed from PANi/TNT-SPCEs. However, a noticeable decrease in the cathodic peaks at −0.2, along with the anodic ones, was observed after the immobilization of anti-SARS-COV-2 and BSA, as shown in Figure 2c. This might have happened because of the presence of more insulating biospecies like anti-SARS-CoV-2 and BSA on the electrode surface. From this observation, a bias voltage of −0.2 V was chosen in general for the subsequent CA analysis as immobilization of antibodies has caused a drastic depletion of the reduction peaks at −0.2 V.

2.2. Chronoamperometric Detection of SARS-CoV-2 and Analytical Performance of the Sensor. According to the procedure described in Figure 4a, a series of CA currents were measured at a bias voltage of −0.2 V, as seen in Figure 2d. It was assumed that SARS-CoV-2 was selectively hybridized with the immobilized anti-SARS-CoV-2 to alter the electrochemical environment of the sensor. It was judged that a change in charge and electron mobility on the PANi-TNT domain has caused the change of sensor voltage to be detected in the potentiostat. It was believed that the distribution of mAb with proper orientation might have played a vital role in capturing the sRBD of SARS-CoV-2 efficiently on the sensor surface.[41]

The average sensor response time was calculated to be less than 2 s, as seen in Figure 2d. The dynamic response (Figure 3a) of the sensor was studied by fitting (four-parameter regression) the current response data against various concentrations of the viral load of SARS-CoV-2 in saliva to evaluate the performance of the sensor. Figure 3b illustrates

https://doi.org/10.1021/acsomega.3c06133
ACS Omega 2023, 8, 45700−45707

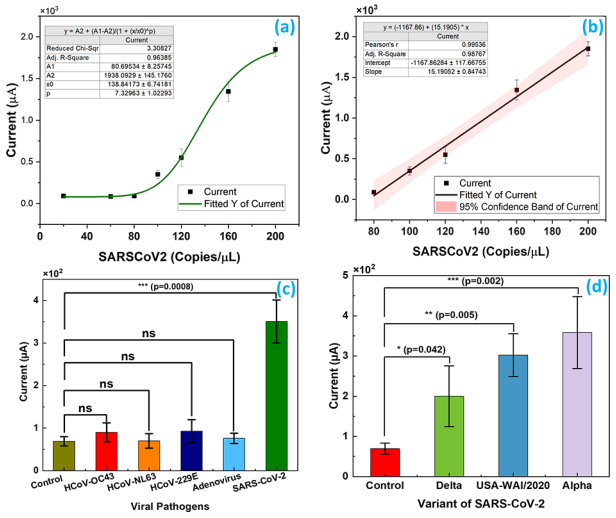

Figure 3. (a) Sensor dose−response curve fitted to the four-parameter regression equation; (b) linearity of the standard curve fitted to linear regression; (c) specificity of the sensor strip toward SARS-CoV-2 in comparison with similar pathogens; (d) performance of the strip toward a different variant of SARS-CoV-2. The asterisk indicates significantly different values compared to the control as determined by the two-tail Student's test (data are expressed as mean ± SEM of three independent experiments; ns = not significant).

the biosensor's linear response (standard curve) with increasing concentrations of SARS-CoV-2. The limit of detection (LOD = 3.3 times the standard deviation of the blank/slope of the linear range) was then calculated from the linear range of 80 to 200 copies/μL to be as low as 25.59 copies/μL.

According to the recently published data, the viral loads of SARS-CoV-2 in clinical samples by RT-PCR ranged from 641 to 1.34×10^{11} copies/mL, with an average of 7.99×10^{4} in throat samples and 7.52×10^{5} in saliva/sputum samples, and 1.69×10^{5} copies/mL for nasal swab samples collected on day 3 after the appearance of symptoms. The average viral load at an early stage was reported below 1×10^{6} copies/mL and 1.34×10^{11} copies/mL detected on day 8 of postonset symptoms in sputum samples collected from COVID-19-suffered dead bodies.[45] By comparison, our biosensor strip's assay LoD of 25.59 copies/μL is lower than the viral load in clinical samples. These results indicated that our assay meets the requirement for sensitivity to diagnose SARS-CoV-2 and could potentially be a candidate to detect in the early stages of illness when the viral load is still low. It is known that many factors can affect test performance and cause false-negative results. Therefore, a solid diagnostic test with high sensitivity could reduce the chances of false negatives caused by low virus recovery from actual samples.

2.3. Specificity Assessment. Optimal electrochemical biosensors should possess the capability to selectively identify and detect the viruses within a sample matrix that includes a variety of biological components such as viruses, enzymes, and proteins. Hence, the sensor's specificity was assessed by contrasting the generated current responses from SARS-CoV-2 with those of other human respiratory viral pathogens, namely, HCoV-OC43, HCoV-NL63, HCoV-229E, and adenovirus. In this test, a known quantity of inactivated viruses (expressed as copies per microliter, copies/μL) was introduced into a saliva matrix. The virus concentration was intentionally maintained at a level at least three times higher than that of SARS-CoV-2, and the experiment was conducted three times to ensure accuracy and consistency of the measurements. As clearly illustrated in Figure 3c, the sensor strip effectively detected SARS-CoV-2 at a concentration of 80 copies/μL, distinguishing it from the higher concentrations (300 copies/μL) of HCoV-OC43, HCoV-NL63, HCoV-229E, and adenovirus.

Statistical analysis was conducted using a two-tailed Student t test to assess the statistical variances among the control group and all the selected pathogens. A significance level of p-value <0.05 was considered as statistically significant. The results showed a high probability of differentiation between SARS-CoV-2 (p = 0.0008) and the other tested pathogens when compared to the control sample, as depicted in Figure 3c. The performance of the strips was further evaluated for different variants of SARS-CoV-2, including delta, USA-WAI/2020, and alpha. The t test analysis indicated the superior ability of the sensor to detect these three variants in the following order: alpha > USA-WAI/2020 > delta, as illustrated in Figure 3d.

The electrochemical interaction of SARS-CoV-2, HCoV-OC43, HCoV-NL63, HCoV-229E, and adenovirus with the surface antibody was also studied by CV scanning in 0.01 M PBS buffer to confirm the specificity of the strips toward SARS-CoV-2. The results revealed that (Figure S5) the strip with SARS-CoV-2 has caused a massive decrease of redox potential, especially the anodic peak in the presence of SARS-CoV-2. On the contrary, strips with HCoV-OC43, HCoV-NL63, HCoV-229E, and adenovirus still showed strong redox peaks. This observation implied that the newly developed sensor strip is highly efficient in specific binding to the S protein of SARS-CoV-2 than that of the other similar groups of viruses.

2.4. Reproducibility and Storage Life Studies. The reproducibility and storage life of the biosensor strips were evaluated by using randomly chosen a set of individual strips. To assess how well the disposable biosensors can be during large production under the same fabrication conditions, a fixed concentration of 150 copies/μL of the inactivated alpha variant of SARS-CoV-2 was tested individually. This study utilized a group of 10 individual single-use strips for analysis. The results revealed a remarkable level of consistency in the production of disposable biosensor strips, as depicted in Figure 4c. Each individual strip demonstrated the ability to generate a similar amount of current during the interaction between antibodies and antigens on the surface. Usually, the sensor strips were stored at 4 °C following their fabrication. The assessment of the strips' relative activity was conducted using a consistent concentration of 150 copies/μL of the inactivated alpha variant of SARS-CoV-2, as illustrated in Figure 4d. As observed, the biosensor maintained approximately 83% of its initial response even after 2 weeks (20th day) since fabrication. This retention in response could be attributed to the denaturation of proteins due to extended storage.

2.5. Clinical Sample Analysis. Finally, the performance of the biosensing strip was evaluated on clinical specimens by taking a fraction of the viral transport media (VTM) with NP swabs collected from COVID-19 patients. Remnants of VTM NP swabs from deidentified clinical specimens with the confirmed qRT-PCR results were used following heat inactivation at 80 °C for 30 min. A 20 μL of heat-inactivated samples (labeled with S1 to S10) was diluted in saliva fluid before testing at BSL-2 facilities according to the procedure described in Figure 4a. The qualitative and quantitative analyses (Figure 4b) demonstrate the confirmation of the

https://doi.org/10.1021/acsomega.3c06133
ACS Omega 2023, 8, 45700−45707

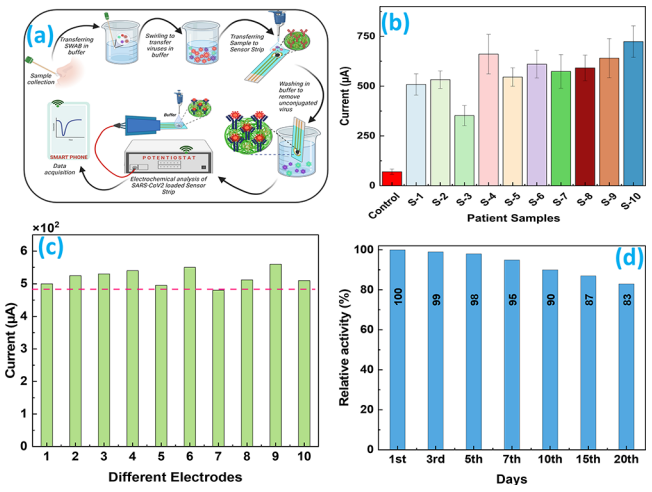

Figure 4. (a) Schematic illustration of sample analysis from collection to data acquisition using the developed strip and portable data reader; (b) performance of the developed electrochemical method to detect SARS-CoV-2 in the nasopharyngeal (NP) swabs of COVID-19 patients; (c) reproducibility of the single-use biosensor strip; (d) storage stability of the strips.

presence of SARS-CoV-2 in all of the samples. The concentration was calculated from the calibration curve ($y = -1167.86 + 15.19x$) (where y is the examined current and x is the copy number) in the range of 110 to 120 copies/μL. Considering the validated findings and the specificity analysis conducted with various viral pathogens (as depicted in Figure 4b), our sensor strip has the capability to identify the presence of SARS-CoV-2 in samples collected from individuals with COVID-19 and effectively distinguish it from other respiratory pathogens.

3. CONCLUSIONS

This report introduces an electrochemical biosensor platform crafted to achieve precise and highly sensitive detection of SARS-CoV-2 by employing SPCE modified with the nanostructure complex of PANi and TNT. The analysis and evaluation of the biosensor strip's performance demonstrate its remarkable linearity in the range of 80 to 200 copies/μL of the target analyte, with a detection limit of as low as 25.59 copies/μL. Moreover, a specificity analysis involving different respiratory viruses like HCoV-OC43, HCoV-NL63, HCoV-229E, and adenovirus highlights the sensor's capacity to discern and selectively identify the spike S protein of SARS-CoV-2. However, the success of a POC platform largely hinges on several factors, including sensitivity, specificity, reproducibility, shelf life, and the stability of the biosensor. Additionally, aspects such as electronic connectivity and data management are crucial for seamless integration into healthcare systems.

In summary, the findings of this study suggest the development of a portable POC-based diagnostic device for the identification and analysis of contagious viruses like SARS-CoV-2 and other respiratory pathogens such as influenza. This diagnostic device is easy to fabricate, rapid to detect, specific to target identification, and noninvasive for sample collection.

4. EXPERIMENTAL SECTION

4.1. Chemicals and Equipment. All chemicals including aniline (Sigma-Aldrich), hydrochloric acid (HCl, Alfa Aesar), acetone (Alfa Aesar), ethanol (Alfa Aesar), bovine serum albumin (BSA, Alfa Aesar), phosphate-buffered saline (PBS, Alfa Aesar), MES buffer (Alfa Aesar), *N*-ethyl-*N*′-3-dimethylaminopropyl-carbodiimide (EDC, Alfa Aesar), *N*-hydroxysuccinimide (NHS, Alfa Aesar), and potassium ferricyanide ($K_3[Fe(CN)_6]$, Alfa Aesar) were of analytical reagent grade and were used as received. Titanium foil (0.25 mm (0.01 in) thick, Alfa Aesar) was used to synthesize TNT. Platinum foil (0.05 mm (0.002 in) thick, Premion, Alfa Aesar) was used as a counter electrode during the anodization of Ti-foil to the synthesis of TNT. A voltage source (Keithley 2400 SourceMeter) was used for anodization. A Mettler Toledo pH meter combined with a pH electrode was used to measure the pH. A PalmSens4 potentiostat (PalmSens, Houten, the Netherlands) with Bluetooth connectivity was used to measure the electrochemical activities including cyclic voltammetry (CV), electrochemical impedance spectroscopy (EIS), and chronoamperometry (CA) of the biosensor. A Quanta FEG 250 scanning electron microscope with FE was used to analyze the morphology of the SPCE before modification by PANi, TNT, and mAb. All solutions with the antibody and viral antigens were prepared in a 0.01 M PBS solution and stored in Eppendorf tubes. In contrast, all other required solutions were prepared in ultrapure water (the Milli-Q Direct 8 system was used to produce). The SARS-CoV-2 spike protein (catalog no. RP-87678) and anti-SARS-CoV-2 mAb (catalog no. MAB38033) were obtained from Thermo Fisher Scientific.

4.2. Fabrication of the Anti-SARS-CoV-2-sRBD-Functionalized Biosensor. *4.2.1. Electrochemical Synthesis of TNT.* TNT was synthesized by our previously reported method with a slight modification.[21] In brief, a size of 2 cm^2 of the Ti sample sheet with a tab 2 mm in width was cut out of a Gl-grade Ti sheet. Both sides of the sheet were polished with 1200 grit polishing paper for 5 min to remove any surface metal oxide layer, followed by sequential sonication in acetone and ethanol for 10 min. The Ti sheet was connected to the voltage source as the WE, and the platinum foil was used as the counter electrode to perform the anodization. Both electrodes were immersed in an electrolyte mixture of ethylene glycol, 0.5 wt % NH_4F, and 5 vol % DI water for 60 min at 30 V. The anodized Ti sheet containing TNT on top was rinsed with ethanol and water. The TNT containing Ti sheet was then annealed at 500 °C for 3 h under an O_2 gas in a tube furnace to convert the phase of TNT from amorphous to crystalline. Next, the TNT containing Ti sheet was sonicated for 30−60 min (depending on the sample size) in 1 M HCl to detach the grown-up TNT from the surface of Ti to the acidic solution. Finally, 0.1 M aniline was dispersed in the acid-containing TNT prior to the electropolymerization on the SPCE.

4.2.2. Modification of the SPCE by PANi and TNT. Commercial SPCE consists of a three-electrode system comprising a carbon WE (d = 4 mm), a carbon counter electrode (CE), and a silver pseudoreference electrode (RE), which were purchased from DropSens (DRP-110, Metrohm DropSens, Oviedo, Spain). To grow a blended PANi-TNT layer on the WE, first, 0.1 M aniline was added with the previously synthesized TNT that is already in an acidic environment. Next, 30 μL of acidic aniline/TNT mixed solution was dropped on the WE, and a CV was run for 5−10 cycles in the voltage window from −0.5 to +1 V at a scan rate of 50 mVs^{-1} at room temperature. A greenish layer (Figure 1c) of PANi appeared on top of the WE after being rinsed with 1 M HCl and DI water to remove any unbound aniline. The

https://doi.org/10.1021/acsomega.3c06133
ACS Omega 2023, 8, 45700−45707

PANi-TNT/SPCE platform is thus ready to be bioconjugated with the capture antibody.

4.2.3. Functionalization of the PANi-TNT/SPCE with Anti-SARS-CoV-2. Immobilization of the mAb anti-SARS-CoV-2 at the surface of the PANi-TNT/SPCE was adopted from elsewhere[46] and is schematically presented in the right panel of Figure 1c. Initially, an EDC and NHS mixture solution with a molar ratio of 1:2 was prepared by dispersion in an Eppendorf tube containing a certain volume of 0.1 M PBS buffer. A calculated amount of two different concentrations of anti-SARS-CoV-2 was added to the mixture solution of EDC/NHS. The mixture was incubated for 30 min to activate the −COOH group of anti-SARS-CoV-2 at room temperature before pipetting a volume of 10 μL on the PANi/TNT modified WE of SPCE. The anti-SARS-CoV-2 attached PANi-TNT/SPCE were then rinsed with PBS buffer at least five times to remove any unbound antibody and unreacted reagent from the surface of sensor strips after 1 h of incubation at 4 °C. Finally, 10 μL of 1% BSA solution was pipetted on all the SPCE and incubated for another 30 min before rinsing with PBS buffer and drying with nitrogen gas to block any nonspecific adsorption sites to have a final biosensor strip configuration as "anti-SARS-CoV-2/PANi-TNT/SPCE".

4.3. Electrochemical Analysis of the Sample. All the electrochemical measurements were conducted using the Bluetooth-enabled potentiostat PalmSens4 (Palm Instruments, the Netherlands). These measurements were carried out in conjunction with either a Windows computer or an Android smartphone at room temperature (25.0 ± 0.5 °C). The potentials were referred to the internal Ag pseudoreference electrode of the SPCE. The electrochemical sensing of SARS-CoV-2 was performed using a freshly fabricated "anti-SARS-CoV-2/PANi-TNT/SPCE"strip connected to a portable potentiostat as shown in the illustration (Figure 4a) and an optical image (Figure S4b,c). To elucidate the analytical performance of the sensor strips, 5 μL of saliva or nasal mucus containing a specific concentration (copies/μL) of SARS-CoV-2 or other pathogens was pipetted on the WE of the strip, incubated for 1−3 min, and flashed with PBS buffer to wash away the unconjugated viruses. Next, a target-virus-loaded strip was connected to a portable potentiostat to record the CA current generated in the presence of a buffer solution as a function of time. It takes less than 30 s to detect the sRBD of SARS-CoV-2 selectively and sensitively on the sensor. However, it needs a maximum of 2−3 min from sample preparation to detection. The obtained current was used to fit the dose−response curve using a logistic equation (four-parameter regression) and a standard curve using linear regression for calculating the LOD.

4.4. Detection of SARS-CoV-2 in Clinical Samples. A fraction of the VTM from COVID-19 patients was collected and stored at −80 °C after diagnostic tests conducted at the Nevada State Public Health Laboratory, Reno, NV, were used to evaluate the performance of the assay. A total of 10 anonymized respiratory clinical samples of positive SARS-CoV-2 were tested to evaluate the detection capability of the strips. The samples were inactivated at 80 °C for 30 min before being analyzed by the developed sensing strips in the biosafety level-2 laboratory (BSL-2).

■ ASSOCIATED CONTENT

Supporting Information

The Supporting Information is available free of charge at https://pubs.acs.org/doi/10.1021/acsomega.3c06133.

Cyclic voltammogram during electropolymerization; additional SEM image of the PANi-SPCE and PANi-TNT/SPCE and antibody-PANi-TNT/SPCE; SEM and EDX data of the PANi-TNT/SPCE; CV after conjugation of SARS-CoV-2, HCoV-OC43, HCoV-NL63, HCoV-229E, and adenovirus on the sensor surface (PDF)

■ AUTHOR INFORMATION

Corresponding Authors

Manoranjan Misra − *Chemical and Materials Engineering Department, University of Nevada, Reno, Nevada 89557, United States*; Email: misra@unr.edu

Subhash C Verma − *Department of Microbiology and Immunology, MS 320, University of Nevada, Reno School of Medicine, Reno, Nevada 89557, United States*; orcid.org/0000-0002-0492-6578; Email: scverma@med.unr.edu

Authors

Al-mahmnur Alam − *Chemical and Materials Engineering Department, University of Nevada, Reno, Nevada 89557, United States*

Timsy Uppal − *Department of Microbiology and Immunology, MS 320, University of Nevada, Reno School of Medicine, Reno, Nevada 89557, United States*

Md Shariful Islam − *Chemical and Materials Engineering Department, University of Nevada, Reno, Nevada 89557, United States*

Complete contact information is available at: https://pubs.acs.org/10.1021/acsomega.3c06133

Author Contributions

A.-M.A., T.U., and M.S.I. did the experimental work, manuscript preparation, and editing. S.C.V. and M.M. reviewed the manuscript.

Funding

This work was supported by Dr. Mick Hitchcock as well as departmental funds (GF06266) of the University of Nevada Reno.

Notes

Patient consent was waived, as the clinical specimens consisting of nasopharyngeal swabs suspended in VTM were deidentified.

The authors declare no competing financial interest.

■ ACKNOWLEDGMENTS

SARS-Related Coronavirus 2—SARS-Related Coronavirus 2, Isolate USA-WA1/2020, Heat Inactivated was deposited by the Centers for Disease Control and Prevention and obtained through BEI Resources, NIAID, NIH: SARS-Related Coronavirus 2, Isolate USA-WA1/2020, Heat Inactivated, NR-52286. SARS-Related Coronavirus 2—Isolate USA/CA_CDC_5574/2020 (Alpha, B.1.1.7), Heat Inactivated was deposited by the Centers for Disease Control and Prevention and obtained through BEI Resources, NIAID, NIH: SARS-Related Coronavirus 2, Isolate USA/CA_CDC_5574/2020, Heat Inactivated, NR-55245. SARS-Related Coronavirus 2—SARS-Related

Coronavirus 2, Isolate hCoV-19/USA/MD-HP05285/2021 (Lineage B.1.617.2; Delta Variant), Heat Inactivated was obtained through BEI Resources, NIAID, NIH: SARS-Related Coronavirus 2, Isolate hCoV-19/USA/MD-HP05285/2021 (Lineage B.1.617.2; Delta Variant), Heat Inactivated, NR-56128. Human coronavirus—NL63 was obtained through BEI Resources, NIAID, NIH: Human Coronavirus, NL63, NR-470. Human Coronavirus—OC43 was obtained through BEI Resources, NIAID, NIH: Human Coronavirus, OC43, NR-52725. Human Coronavirus—229E was obtained through BEI Resources, NIAID, NIH: Human Coronavirus, 229E, NR-52726. Adenovirus Serotype 5, Clone Ad5 was obtained through BEI Resources, NIAID, NIH: Adenovirus Serotype 5, Clone Ad5-CMV-hACE2/RSV-eGFP, Recombinant Expressing Human ACE2, NR-52390.

REFERENCES

(1) Tao, S.; Zhao, X.; Bao, D.; Liu, X.; Zhang, W.; Zhao, L.; Tang, Y.; Wu, H.; Ye, H.; Yang, Y.; Deng, D. SARS-CoV-2 Spike-S1 Antigen Test Strip with High Sensitivity Endowed by High-Affinity Antibodies and Brightly Fluorescent QDs/ Silica Nanospheres. *ACS Appl. Mater. Interfaces* **2023**, *15*, 27612−27623.

(2) Dong, Y.; Zhao, Y.; Li, S.; Wan, Z.; Lu, R.; Yang, X.; Yu, G.; Reboud, J.; Cooper, J. M.; Tian, Z.; Zhang, C. Multiplex, Real-time, Point-of-Care RT-LAMP for SARS-CoV-2 Detection Using the HFman Probe. *ACS Sens.* **2022**, *7* (3), 730−739.

(3) https://www.cdc.gov/coronavirus/2019ncov/lab/naats.html.

(4) Cho, S.; Jin, X.; Gong, X.; Yang, S.; Cui, J.; Strano, M. S. Antibody-Free Rapid Detection of SARS-CoV-2 Proteins Using Corona Phase Molecular Recognition to Accelerate Development Time. *Anal. Chem.* **2021**, *93* (44), 14685−14693.

(5) Esbin, M. N.; Whitney, O. N.; Chong, S.; Maurer, A.; Darzacq, X.; Tjian, R. Overcoming the Bottleneck to Widespread Testing: A Rapid Review of Nucleic Acid Testing Approaches for COVID-19 Detection. *RNA* **2020**, *26*, 771−783.

(6) Mio, C.; Cifù, A.; Marzinotto, S.; Bergamin, N.; Caldana, C.; Cattarossi, S.; Cmet, S.; Cussigh, A.; Martinella, R.; Zucco, J.; Verardo, R.; Schneider, C.; Marcon, B.; Zampieri, S.; Pipan, C.; Curcio, F.; Liu, Z. A Streamlined Approach to Rapidly Detect SARS-CoV-2 Infection Avoiding RNA Extraction: Workflow Validation. *Dis. Markers* **2020**, *2020*, No. 8869424.

(7) McMinn, S.; Carlsen, A.; Jaspers, B.; Talbot, R.; Adeline, S. In Large Texas Cities, Access to Coronavirus Testing May Depend on Where You Live. https://www.npr.org/sections/health-shots/2020/05/27/862215848/across-texas-black-and-hispanic-neighborhoods-havefewer-coronavirus-testing-sit 2020.

(8) Yao, C. Y.; Fu, W. L. Biosensors for Hepatitis B Virus Detection. *World J. Gastroenterol* **2014**, *20*, 12485−12492.

(9) Nidzworski, D.; Siuzdak, K.; Niedziałkowski, P.; Bogdanowicz, R.; Sobaszek, M.; Ryl, J.; Weiher, P.; Sawczak, M.; Wnuk, E.; Goddard, W. A.; Jaramillo-Botero, A.; Ossowski, T. A Rapid-Response Ultrasensitive Biosensor for Influenza Virus Detection Using Antibody-Modified Boron-Doped Diamond. *Sci. Rep.* **2017**, *7*, 1−10.

(10) Malhotra, B. D.; Ali, M. A. Chapter 1 - Nanomaterials in Biosensors: Fundamentals and Applications, In *Micro and Nano Technologies, Nanomaterials for Biosensors*; William Andrew Publishing 2018; pp 1−74 DOI: 10.1016/B978-0-323-44923-6.00001-7.

(11) Grieshaber, D.; MacKenzie, R.; Vörös, J.; Reimhult, E. Electrochemical Biosensors - Sensor Principles and Architectures. *Sensors* **2008**, *8*, 1400−1458.

(12) Parihar, A.; Ranjan, P.; Sanghi, S. K.; Srivastava, A. K.; Khan, R. Point-of-Care Biosensor-Based Diagnosis of COVID-19 Holds Promise to Combat Current and Future Pandemics. *ACS Appl. Bio Mater.* **2020**, *3* (11), 7326−7343.

(13) Estrela, P.; Bhalla, N.; Jolly, P.; Formisano, N. Introduction to Biosensors. *Essays Biochem.* **2016**, *60* (1), 1−8.

(14) Altug, H.; Oh, S. H.; Maier, S. A.; Homola, J. Advances and Applications of Nanophotonic Biosensors. *Nat. Nanotechnol.* **2022**, *17*, 5−16.

(15) Sadique, M. A.; Yadav, S.; Ranjan, P.; Khan, R.; Khan, F.; Kumar, A.; Biswas, D. Highly Sensitive Electrochemical Immunosensor Platforms for Dual Detection of SARS-CoV-2 Antigen and Antibody Based on Gold Nanoparticle Functionalized Graphene Oxide Nanocomposites. *ACS Appl. Bio Mater.* **2022**, *5* (5), 2421−2430.

(16) Yadav, S.; Abubakar Sadique, M.; Ranjan, P.; Khan, R.; Sathish, N.; Srivastava, A. K. Polydopamine Decorated MoS 2 Nanosheet Based Electrochemical Immunosensor for Sensitive Detection of SARS-CoV-2 Nucleocapsid Protein in Clinical Samples. *J. Mater. Chem. B* **2022**, *10*, 8478−8489.

(17) Yadav, S.; Sadique, M. A.; Ranjan, P.; Khan, R. Synergistically Functionalized Molybdenum Disulfide-Reduced Graphene Oxide Nanohybrid Based Ultrasensitive Electrochemical Immunosensor for Real Sample Analysis of Covid-19. *Anal. Chim. Acta* **2023**, *1265*, No. 341326.

(18) Sadique, M. A.; Yadav, S.; Khare, V.; Khan, R.; Tripathi, G. K.; Khare, P. S. Functionalized Titanium Dioxide Nanoparticle-Based Electrochemical Immunosensor for Detection of SARS-CoV-2 Antibody. *Diagnostics* **2022**, *12* (11), 2612.

(19) Vadlamani, B. S.; Uppal, T.; Verma, S. C.; Misra, M. Functionalized TiO_2 Nanotube-Based Electrochemical Biosensor for Rapid Detection of SARS-CoV-2. *Sensors* **2020**, *20*, 5871.

(20) Bhattacharyya, D.; Smith, Y. R.; Mohanty, S. K.; Misra, M. Titania Nanotube Array Sensor for Electrochemical Detection of Four Predominate Tuberculosis Volatile Biomarkers. *J. Electrochem. Soc.* **2016**, *163*, B206−B214.

(21) Smith, Y. R.; Bhattacharyya, D.; Mohanty, S. K.; Misra, M. Anodic Functionalization of Titania Nanotube Arrays for the Electrochemical Detection of Tuberculosis Biomarker Vapors. *J. Electrochem. Soc.* **2016**, *163*, B83−B89.

(22) Chin, S. F.; Lim, L. S.; Pang, S. C.; Sum, M. S. H.; Perera, D. Carbon Nanoparticle Modified Screen-Printed Carbon Electrode as a Disposable Electrochemical Immunosensor Strip for the Detection of Japanese Encephalitis Virus. *Microchim. Acta* **2017**, *184*, 491−497.

(23) Siuzdak, K.; Niedziałkowski, P.; Sobaszek, M.; Łęga, T.; Sawczak, M.; Czaczyk, E.; Dziąbowska, K.; Ossowski, T.; Nidzworski, D.; Bogdanowicz, R. Biomolecular Influenza Virus Detection Based on the Electrochemical Impedance Spectroscopy Using the Nanocrystalline Boron-Doped Diamond Electrodes with Covalently Bound Antibodies. *Sens. Actuators, B* **2019**, *280*, 263−271.

(24) Lee, T.; Park, S. Y.; Jang, H.; Kim, G. H.; Lee, Y.; Park, C.; Mohammadniaei, M.; Lee, M. H.; Min, J. Fabrication of Electrochemical Biosensor Consisted of Multi-Functional DNA Structure/Porous Au Nanoparticle for Avian Influenza Virus (H5N1) in Chicken Serum. *Mater. Sci. Eng. C* **2019**, *99*, 511−519.

(25) Singhal, C.; Dubey, A.; Mathur, A.; Pundir, C. S.; Narang, J. Paper-Based DNA Biosensor for Detection of Chikungunya Virus Using Gold Shells Coated Magnetic Nanocubes. *Process Biochem.* **2018**, *74*, 35−42.

(26) Sayhi, M.; Ouerghi, O.; Belgacem, K.; Arbi, M.; Tepeli, Y.; Ghram, A.; Anik, Ü.; Österlund, L.; Laouini, D.; Diouani, M. F. Electrochemical Detection of Influenza Virus H9N2 Based on Both Immunomagnetic Extraction and Gold Catalysis Using an Immobilization-Free Screen-Printed Carbon Microelectrode. *Biosens. Bioelectron.* **2018**, *107*, 170−177.

(27) Singh, R.; Hong, S.; Jang, J. Label-Free Detection of Influenza Viruses Using a Reduced Graphene Oxide-Based Electrochemical Immunosensor Integrated with a Microfluidic Platform. *Sci. Rep.* **2017**, *7*, 1−11.

(28) Gao, Z.; Li, Y.; Zhang, X.; Feng, J.; Kong, L.; Wang, P.; Chen, Z.; Dong, Y.; Wei, Q. Ultrasensitive Electrochemical Immunosensor for Quantitative Detection of HBeAg Using Au@Pd/MoS_2@MWCNTs nanocomposite as enzyme-mimetic labels. *Biosens. Bioelectron.* **2018**, *102*, 189−195.

https://doi.org/10.1021/acsomega.3c06133
ACS Omega 2023, 8, 45700−45707

(29) Ghanbari, K.; Roushani, M. A Nanohybrid Probe Based on Double Recognition of an Aptamer MIP Grafted onto an MWCNTs-Chit Nanocomposite for Sensing Hepatitis C Virus Core Antigen. *Sens. Actuators B: Chem.* **2018**, *258*, 1066−1071.
(30) Zhang, X.; Qi, Q.; Jing, Q.; Ao, S.; Zhang, Z.; Ding, M.; Wu, M.; Liu, K.; Wang, W.; Ling, Y.; Zhang, Z.; Fu, W. Electrical Probing of COVID-19 Spike Protein Receptor Binding Domain via a Graphene Field-Effect Transistor. *arXiv* **2020**, *2003*, 12529.
(31) McClements, J.; Bar, L.; Singla, P.; Canfarotta, F.; Thomson, A.; Czulak, J.; Johnson, R. E.; Crapnell, R. D.; Banks, C. E.; Payne, B.; Seyedin, S.; Losada-Pérez, P.; Peeters, M. Molecularly Imprinted Polymer Nanoparticles Enable Rapid, Reliable, and Robust Point-of-Care Thermal Detection of SARSCoV 2. *ACS Sens.* **2022**, *7*, 1122−1131.
(32) Kasetsirikul, S.; Umer, M.; Soda, N.; Sreejith, R. K.; Shiddiky, M. J. A.; Nguyen, N. Detection of the SARS-CoV-2 Humanized Antibody with Paper-Based ELISA. *Analyst* **2020**, *145*, 7680.
(33) Zhang, T.; Sun, L.; Zhang, Y. Highly Sensitive Electrochemical Determination of the SARS-COV-2 Antigen Based on a Gold/Graphene Imprinted Poly-Arginine Sensor. *Anal. Methods* **2021**, *13*, 5772.
(34) Zeng, R.; Qiu, M.; Wan, Q.; Huang, Z.; Liu, X.; Tang, D.; Knopp, D. Smartphone-Based Electrochemical Immunoassay for Point-of-Care Detection of SARS-CoV 2 Nucleocapsid Protein. *Anal. Chem.* **2022**, *94*, 15155−15161.
(35) Perdomo, S. A.; Ortega, V.; Jaramillo-Botero, A.; Mancilla, N.; Mosquera-DeLaCruz, J. H.; Valencia, D. P.; Quimbaya, M.; Contreras, J. D.; Velez, G. E.; Loaiza, O. A.; Gomez, A.; de la Roche, J. SenSARS: A Low-Cost Portable Electrochemical System for Ultra-Sensitive, Near Real-Time, Diagnostics of SARS-CoV-2 Infections. *IEEE Trans. Instrum. Meas.* **2021**, *70*, No. 4007710.
(36) Abrego-Martinez, J. C.; Jafari, M.; Chergui, S.; Pavel, C.; Che, D.; Sia, M. Aptamer-based electrochemical biosensor for rapid detection of SARS-CoV-2: Nanoscale Electrode-Aptamer-SARS-CoV-2 Imaging by Photo-Induced Force Microscopy. *Biosens. Bioelectron.* **2022**, *195*, No. 113595.
(37) Drobysh, M.; Ramanavicius, A.; Baradoke, A. Polyaniline-Based Electrochemical Immunosensor for the Determination of Antibodies against SARS-CoV-2 Spike Protein. *Sci. Total Environ.* **2023**, *862*, No. 160700.
(38) Samper, I. C.; McMahon, C. J.; Schenkel, M. S.; Clark, K. M.; Khamcharoen, W.; Anderson, L. B. R.; Terry, J. S.; Gallichotte, E. N.; Ebel, G. D.; Geiss, B. J.; Dandy, D. S.; Henry, C. S. Electrochemical Immunoassay for the Detection of SARS-CoV 2 Nucleocapsid Protein in Nasopharyngeal Samples. *Anal. Chem.* **2022**, *94*, 4712−4719.
(39) Mondol, P.; Barile, C. J. Four-Electron Electrocatalytic O_2 Reduction by a Ferrocene-Modified Glutathione Complex of Cu. *ACS Appl. Energy Mater.* **2021**, *4*, 9611−9617.
(40) Mondol, P.; Thind, J. K.; Barile, C. J. Selective Electrocatalytic Nitrate Reduction to Ammonia Using Nafion-Covered Cu Electrodeposits. *J. Phys. Chem. C* **2023**, *127*, 8054−8061.
(41) Acosta-Alejandro, J. A.; López-González, R.; Frías-Márquez, D. M.; De La Rosa-Vázquez, J. M.; Uribe-López, M. C.; Gómez, R. Polyaniline-Sensitized SiO_2/TiO_2 Photocatalysts for the Degradation of Phenol Using Visible Light. *J. Photochem. Photobiol., A* **2022**, *425*, No. 113696.
(42) Smith, S.; Goodge, K.; Delaney, M.; Struzyk, A.; Tansey, N.; Frey, M. A Comprehensive Review of the Covalent Immobilization of Biomolecules onto Electrospun Nanofibers. *Nanomaterials (Basel).* **2020**, *10* (11), 2142.
(43) Mondol, P.; Panthi, D.; Albarran Ayala, A. J.; Odoh, S. O.; Barile, C. J. Membrane-Modified Electrocatalysts for Nitrate Reduction to Ammonia with High Faradaic Efficiency. *J. Mater. Chem. A* **2022**, *10*, 22428.
(44) Guo, S.; Lakshmipriya, T.; Gopinath, S. C. B.; Anbu, P.; Feng, Y. Complementation of ELISA and an Interdigitated Electrode Surface in Gold Nanoparticle Functionalization for Effective Detection of Human Blood Clotting Defects. *Nanoscale Res. Lett.* **2019**, *14*, 222.
(45) Gao, S.; Guisán, J. M.; Rocha-Martin, J. Oriented Immobilization of Antibodies onto Sensing Platforms - A Critical Review. *Anal. Chim. Acta* **2022**, *1189*, No. 338907.
(46) Lv, H.; Wang, Y.; Pan, L.; Zhang, L.; Zhang, H.; Shang, L.; Qu, H.; Li, N.; Zhao, J.; Li, Y. Patterned Polyaniline Encapsulated in Titania Nanotubes for Electrochromism. *Phys. Chem. Phys. Chem.* **2018**, *20*, 5818−5826.

https://doi.org/10.1021/acsomega.3c06133
ACS Omega 2023, 8, 45700−45707